Journal of Materials Chemistry

Cite this: J. Mater. Chem., 2012, 22, 22224

www.rsc.org/materials

PAPER

New TIPS-substituted benzo[1,2-*b*:4,5-*b*′]dithiophene-based copolymers for application in polymer solar cells†

Chinna Bathula,‡[a] Chang Eun Song,‡[b] Sachin Badgujar,[ac] Seong-Jin Hong,[ac] In-Nam Kang,[d] Sang-Jin Moon,[a] Jaemin Lee,[a] Shinuk Cho,*[e] Hong-Ku Shim*[f] and Sang Kyu Lee*[ac]

Received 30th May 2012, Accepted 6th September 2012
DOI: 10.1039/c2jm33466f

Novel triisopropylsilylethynyl (TIPS)-substituted benzodithiophene-based copolymers, poly[4,8-bis(triisopropylsilylethynyl)benzo[1,2-*b*:4,5-*b*′]dithiophene-2,6-diyl-*alt*-4,6-(2-ethylhexyl-thieno[3,4-*b*]thiophene-2-carboxylate)] (**P1**), poly[4,8-bis(triisopropylsilylethynyl)benzo[1,2-*b*:4,5-*b*′]dithiophene-2,6-diyl-*alt*-[4,6-{(1-thieno[3,4-*b*]thiophen-2-yl)-2-ethylhexan-1-one}] (**P2**), and poly[4,8-bis(triisopropylsilylethynyl)benzo[1,2-*b*:4,5-*b*′]dithiophene-2,6-diyl-*alt*-4,6-(2-ethylhexyl(3-fluorothieno[3,4-*b*]thiophene)-2-carboxylate)] (**P3**), were designed and synthesized for use in polymer solar cells (PSCs). We describe the effects of the different acceptor segment side groups on the optical, electrochemical, field-effect hole mobility, and photovoltaic characteristics of the resulting TIPS-based copolymers. The side groups in the copolymers were found to significantly influence the carrier mobilities and photovoltaic properties of the copolymers. The field-effect mobilities of the holes varied from 9×10^{-5} cm^2 V^{-1} s^{-1} in **P2** to 3×10^{-3} cm^2 V^{-1} s^{-1} in **P1**. Under optimized conditions, the TIPS-based polymers showed power conversion efficiencies (PCEs) for the PSCs in the range of 3.16–5.76%. Among the TIPS-based copolymers studied here, **P1** showed the best photovoltaic performance, with an open-circuit voltage (V_{oc}) of 0.82 V, a short-circuit current density (J_{sc}) of 12.75 mA cm^{-2}, a fill factor (FF) of 0.55, and a power-conversion efficiency of 5.76% using a **P1**:$PC_{71}BM$ blend film as the active layer under AM 1.5G irradiation (100 mW cm^{-2}).

Introduction

Recently, polymer solar cells (PSCs) based on blends of conjugated polymers and fullerene derivatives have gained considerable attention as a means for harvesting renewable clean solar energy because of their unique advantages, including their low cost, light weight, solution processability, and flexibility.[1–10] Significant efforts have been applied toward improving the power conversion efficiencies (PCEs) of PSCs. The PCEs of PSCs have reached 7–8%, primarily due to the development of new low band gap polymers and better control over the nanoscale morphologies of the interpenetrating electron donor–acceptor networks.[11,12]

The decisive parameters that determine the PSC efficiency are the open-circuit voltage (V_{oc}), short-circuit current (J_{sc}), and fill factor (FF). V_{oc} is limited by the difference between the highest occupied molecular orbital (HOMO) of the donor and the lowest unoccupied molecular orbital (LUMO) of the acceptor.[13,14] J_{sc} and FF are directly limited by the charge carrier mobility. Higher charge carrier mobilities enable better carrier transport within an active layer without significant photocurrent loss due to recombination of opposite charges.[15,16] Maximization of the short-circuit current requires a planar structure to encourage the crystallinity of the polymer.[17,18] The introduction of more rigid planar structural moieties in conjugated polymers has been shown to be an effective approach to minimize the phase separation because the coplanar structures benefit from improved π–π stacking of the copolymers in the solid state.[19–21]

Recently, we reported a new class of triisopropylsilylethynyl (TIPS) group-substituted anthracene-based copolymers, **PAT2** and **PAT4**, that displayed an extended π-conjugation length and yielded improved charge transport properties.[22] The hole mobility of **PAT4** was high, up to 0.037 cm^2 V^{-1} s^{-1}. **PAT4** displayed a very good absorbance and a promising PCE of 1.7%;

[a]*Energy Materials Research Center, Korea Research Institute of Chemical Technology (KRICT), 141 Gajeong-ro, Yuseong-gu, Daejeon, 305-600, Korea. E-mail: skyulee@krict.re.kr*
[b]*Department of Materials Science and Engineering, Korea Advanced Instituted of Science and Technology, Daejeon, 305-701, Korea*
[c]*Nanomaterials Science and Engineering Major, University of Science and Technology (UST), 217 Gajeong-ro, Yuseong-gu, Daejeon, Korea*
[d]*Department of Chemistry, The Catholic University of Korea, Bucheon, Gyeonggi-do, 420-743, Korea*
[e]*Department of Physics and EHSRC, University of Ulsan, Ulsan 680-749, Korea. E-mail: sucho@ulsan.ac.kr*
[f]*Department of Chemistry, Korea Advanced Instituted of Science and Technology, Daejeon, 305-701, Korea. E-mail: hkshim@kaist.ac.kr*

† Electronic supplementary information (ESI): TGA data, UPS data, SCLC data, and the performance of the PSCs under various conditions. See DOI: 10.1039/c2jm33466f

‡ C. Bathula and C. E. Song contributed equally to this work.

however, the pendant chains on the thiophene unit of **PAT2** gave rise to steric interactions and a coplanar polymer backbone, resulting in a poor molecular weight and altered optical and electrochemical properties relative to the TIPS-anthracene-based copolymers. Zhan *et al.* reported TIPS substituted benzodithiophene-based copolymers containing thiazolothiazole acceptor units with a power conversion efficiency of 4.33%.[23] A new polymer backbone was needed to overcome the solubility, steric hindrance, and band gap problems.

In this study, poly[4,8-bis(triisopropylsilylethynyl)benzo[1,2-*b*:4,5-*b*′]dithiophene-2,6-diyl-*alt*-4,6-(2-ethylhexyl-thieno[3,4-*b*]thiophene-2-carboxylate)] (**P1**), poly[4,8-bis(triisopropylsilylethynyl)-benzo[1,2-*b*:4,5-*b*′]dithiophene-2,6-diyl-*alt*-[4,6-{(1-thieno[3,4-*b*]thiophen-2-yl)-2-ethylhexan-1-one}] (**P2**), and poly[4,8-bis-(triisopropylsilylethynyl)benzo[1,2-*b*:4,5-*b*′]dithiophene-2,6-diyl-*alt*-4,6-(2-ethylhexyl(3-fluorothieno[3,4-*b*]thiophene)-2-carboxylate)] (**P3**), which have the same polymer backbone but different side chains, were designed and synthesized to achieve a higher PCE. The steric hindrance and solubility problems of **PAT2** were ameliorated here by replacing the bithiophene units of the thieno[3,4-*b*]thiophene derivatives with various electron-withdrawing functional groups, which acted as a donor–acceptor system. We also replaced the anthracene groups with benzo[1,2-*b*:4,5-*b*′]dithiophene (BDT) units. We attempted to synthesize a TIPS group-substituted anthracene-based copolymer by polycondensation of 2,6-bis(trimethyltin)-9,10-bis(triisopropylsilylethynyl)anthracene and the corresponding dibrominated thieno[3,4-*b*]thiophene derivatives for the purpose of using the reference; however, the TIPS group-substituted anthracene-based copolymer was obtained as a sticky liquid that was difficult to purify. We expected that the introduction of BDT units would improve the optical properties, including the band gap and the hole mobility. We systematically investigated the synthesis, thermal stability, optical and electrochemical properties, field-effect carrier mobilities, and photovoltaic characteristics of the resulting polymers. Bulk heterojunction PSCs prepared from **P1** produced a PCE of 5.76% under 100 mW cm^{-2} AM 1.5 G irradiation in ambient air.

Results and discussion

Synthesis and characterization of the polymers

The synthetic routes for preparing the TIPS-BDT-based polymers are shown in Scheme 1. Three types of BDT-based copolymers were synthesized by polycondensation of 2,6-bis(trimethyltin)-4,8-bis(triisopropylsilylethynyl)-benzo[1,2-*b*:4,5-*b*′]dithiophene and the corresponding dibrominated thieno[3,4-*b*]thiophene derivatives through the palladium-catalyzed Stille reaction. The crude polymers were extracted with chloroform, collected by precipitating them in methanol, and extracted with methanol and acetone, successively, using a Soxhlet apparatus to remove byproducts and oligomers. The molecular weights were determined by gel permeation chromatography (GPC) against polystyrene standards in a chloroform eluent and were found to be in the range of 11–19 kDa with a polydispersity index of 1.7–2.2 (Table 1).

The thermal properties of the copolymers under a nitrogen atmosphere, characterized by thermogravimetric analysis (TGA) at a heating rate of 10 °C min^{-1}, yielded decomposition temperatures (T_d) in the range of 360–420 °C. The physical properties of the polymers are summarized in Table 1.

Optical properties

The UV-vis absorption spectra of the polymers in chloroform and in the spin-coated films are shown in Fig. 1 and 2, respectively, and the corresponding absorption properties are summarized in Table 2. In the chloroform solvent, all polymers exhibited similar absorption spectra. The UV-vis absorption maxima of **P1**, **P2**, and **P3** occurred at 641, 648, and 628 nm, respectively, in solution, and at 678, 677, and 669 nm, respectively, in the film state. The absorption maxima of the polymer films were red-shifted by 29–41 nm compared with the maxima of the polymers in solution. The red shift indicated a higher polymer coplanarity and/or enhanced intermolecular electronic interactions in the solid state. The red shift observed for **P1** and **P3** was larger than that of **P2** due to the structural changes in the side chain induced by the ketone group (**P2**) and the ester group (**P1**). These effects were investigated by performing theoretical calculations using density functional theory (DFT) with the DMol 3 software. The computational study was conducted by selecting several repeating units as simplified models (two repeating units). Fig. 3 depicts the electron state density distribution of the HOMO and LUMO of the geometry-optimized structures of the polymers. The results predicted that the HOMO was delocalized over the polymer backbone, whereas the LUMO was almost localized at the electron-acceptor site. This configuration is generally observed for low band gap polymers with push–pull units.[8,24] The dihedral angles between the BDT units and the thieno[3,4-*b*]thiophene units were significant, as can be seen from the calculated structures (Fig. 3). The torsional angles of **P1** and **P3** were smaller than those of **P2**. The resulting red shift observed for **P1** and **P3**, compared with **P2**, arose from the minimal coplanarity of the polymer backbone with the ester group substitution.

The absorption maxima of the fluorinated polymer, **P3**, were blue shifted by 10 nm relative to the maxima of the unfluorinated polymer, **P1**. As previously reported, the introduction of more electron-withdrawing fluorine groups to the polymer backbone blue-shifted the polymer absorption maxima.[25] The optical band gap obtained from the extrapolation of the absorption edges of the film followed the ordering **P2** (1.67 eV) < **P1** (1.69 eV) < **P3** (1.71 eV).

Electrochemical properties

The energy levels of the HOMO and LUMO were determined by measuring the electrochemical properties of the polymers using cyclic voltammetry (CV). A platinum (Pt) electrode was modified with a polymer film by means of dip-coating, and was used as the working electrode. A Pt wire was used as the counter electrode, and $Ag/AgNO_3$ (0.10 M) served as the reference electrode. The CV measurements were carried out in a tetrabutylammonium tetrafluoroborate ($TBABF_4$, 0.1 M)/acetonitrile electrolyte at room temperature under a nitrogen atmosphere at a scan rate of 50 mV s^{-1}. Fig. 4 shows the oxidation cyclic voltammograms of the polymers. The HOMO level of the polymers was deduced

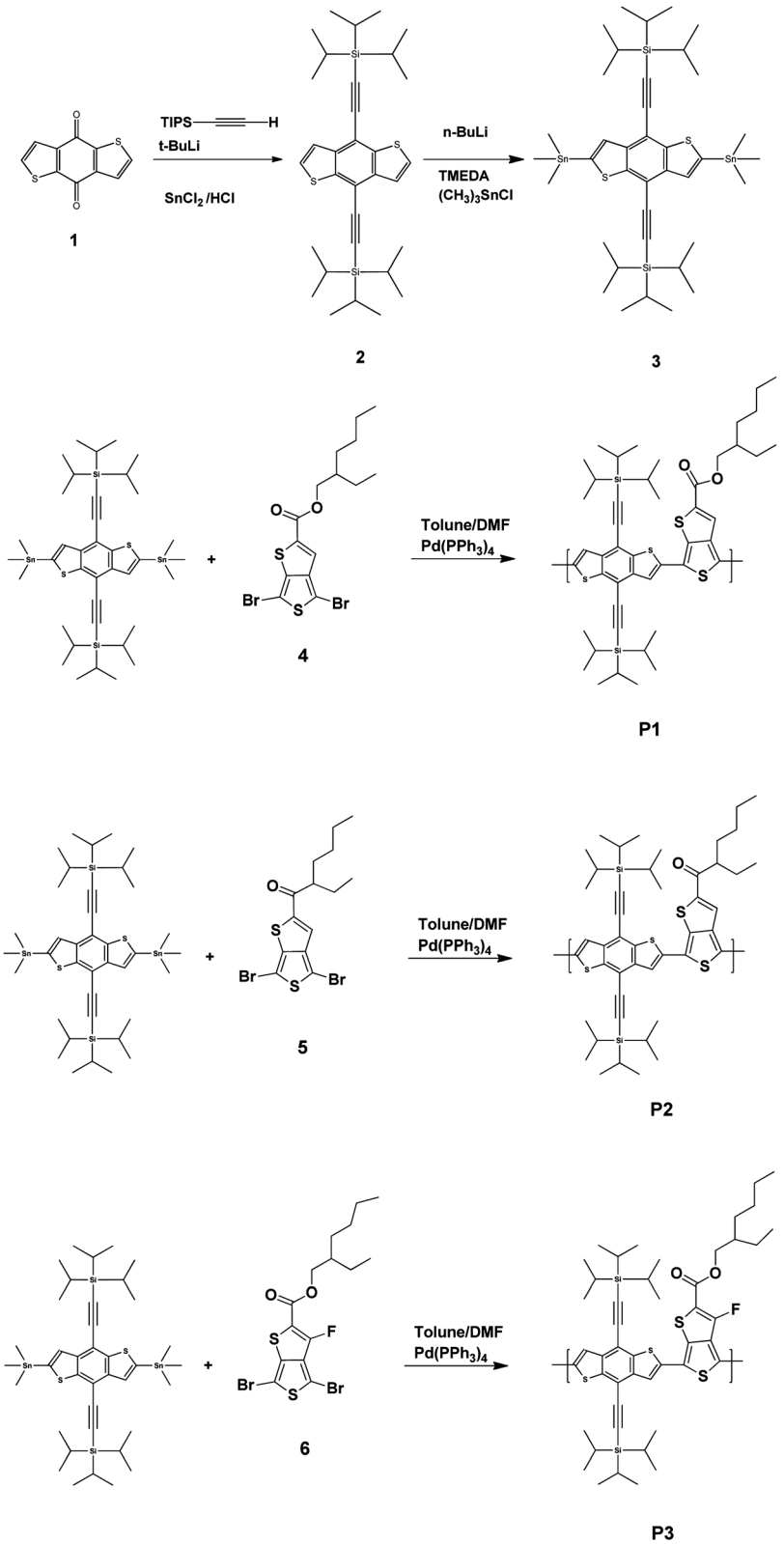

Scheme 1 Synthetic scheme for the monomer and copolymers.

based on the oxidation onsets under the assumption that the energy level of ferrocene (Fc) was 4.8 eV below the vacuum level.[26] In the anodic scan, the onset of oxidation for **P1**, **P2**, and **P3** occurred at 0.80, 0.81, and 0.80 V, corresponding to ionization potential values of −5.60, −5.61, and −5.60 eV, respectively. As expected from the structures of the polymers, polymers with identical backbone structures had similar HOMO energy values.

Table 1 Physical properties of the polymers

Polymer	M_n[a] [kg mol^{-1}]	PDI	Yield (%)	T_d[b] (°C)
P1	11	1.9	85	372
P2	19	2.2	84	420
P3	11	1.7	87	360

[a] The molecular weights were determined by using gel permeation chromatography (GPC) against polystyrene standards in chloroform eluent. [b] Temperature resulting in 5% weight loss based on initial weight.

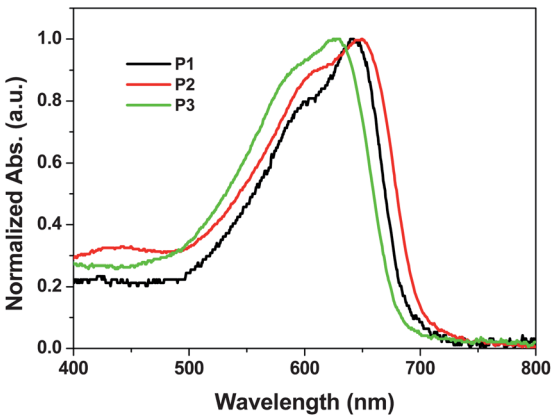

Fig. 1 UV-Vis absorption spectra of the copolymers in chloroform solutions.

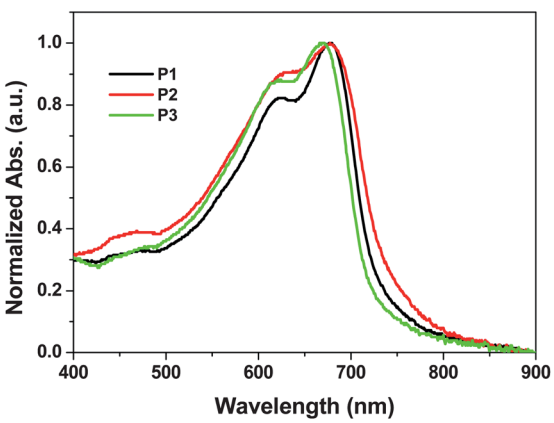

Fig. 2 UV-Vis absorption spectra of thin films of the copolymers.

Table 2 Optical and electrochemical properties of the polymers

Polymer	$\lambda_{max}^{abs,sol}$[a] (nm)	$\lambda_{max}^{abs,film}$[a] (nm)	HOMO[b] (eV)	LUMO[c] (eV)	E_g^{opt}[d] (eV)
P1	641	678	−5.60	−3.91	1.69
P2	648	677	−5.61	−3.94	1.67
P3	628	669	−5.60	−3.89	1.71

[a] The UV-Vis absorption spectra of the polymers were measured in chloroform solution and thin film. [b] HOMO levels of the polymer were determined from onset voltage of the first oxidation potential with reference to ferrocene at −4.8 eV. [c] LUMO levels of the polymer were estimated from the optical band gaps and the HOMO energies. [d] Optical band gap calculated from the UV-Vis absorption onset in film.

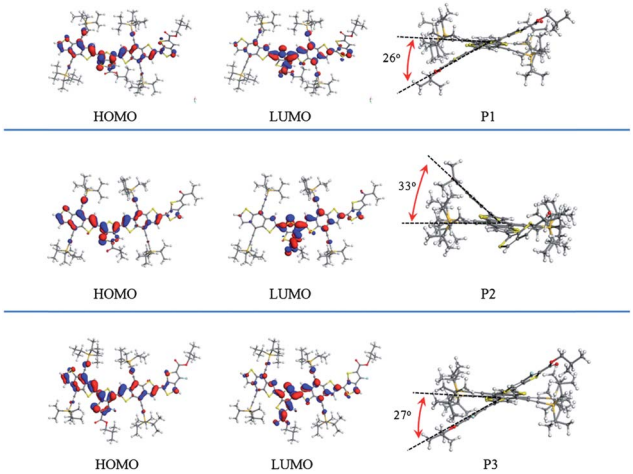

Fig. 3 DFT-optimized geometries and charge density isosurfaces of the HOMO and LUMO levels, and side views of the thiophenyl BDT-based polymers.

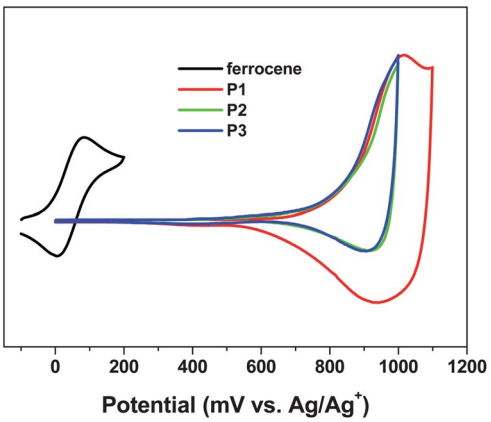

Fig. 4 Cyclic voltammograms of the copolymers.

The LUMO energies of the copolymers were estimated based on the optical band gaps (determined from the absorption onsets in the UV-vis spectra of the polymers films) and the HOMO energies. The energies of the LUMO levels of **P1**, **P2**, and **P3** are listed in Table 2. No fluorine effects were observed in the electrochemical properties. Any inter- or intra-chain interaction may also influence the HOMO level. The dihedral angle between the bulky TIPS-BDT units and the thienothiophene units is significant, as can be seen from the calculated structures (Fig. 3). The dihedral angle for **P1** without the fluorine unit is very similar to that for **P3** with the fluorine unit. We guess that steric hindrance between the bulky TIPS-BDT units and the thienothiophene units significantly affects the coplanar structure of the polymers. For this reason, we think that not the fluorine effect but the interaction between the bulky TIPS-BDT units and the thienothiophene units exerted an important effect on optical properties as well as electrochemical properties.

Field-effect transistor characteristics

The effects of the side chain substitutions on the electrical transport properties of the resulting materials were examined by measuring the mobilities of each of the three copolymers. The

field-effect carrier mobilities of the polymers were investigated by fabricating thin film transistors (TFTs) with a bottom-contact geometry using Au electrodes. The device fabrication process is described in detail in the Experimental section. A high charge-carrier mobility (comparable to or exceeding 10^{-3} cm^2 V^{-1} s^{-1}) was necessary to reduce the photocurrent loss and obtain high-performance PSC devices.[27,28] Fig. 5 shows the transfer curves for the polymers. The TFTs of the polymers were found to exhibit typical p-channel TFT characteristics. The TFT mobilities were calculated in the saturation region using the following equation:[29]

$$I_{ds} = (WC_i/2L)\mu(V_G - V_T)^2,$$

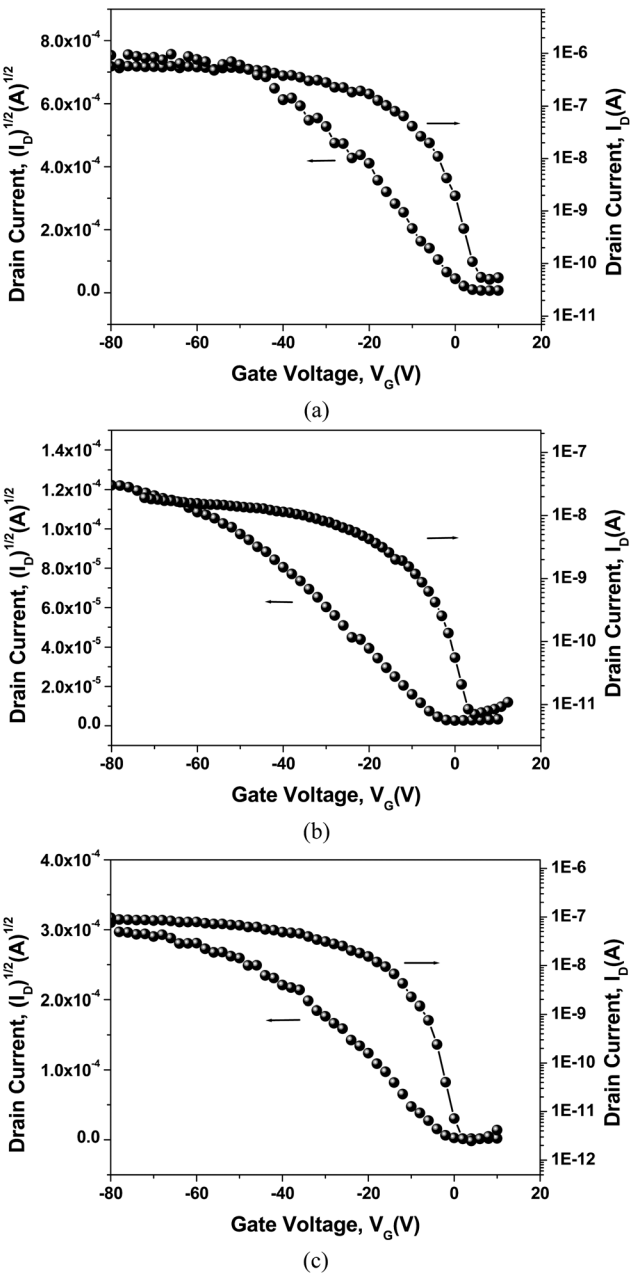

Fig. 5 Transfer characteristics of an OFET fabricated from **P1** (a), **P2** (b), and **P3** (c).

where I_{ds} is the drain-source current in the saturated region, W and L are the channel width (120 μm) and length (12 μm), respectively, μ is the field-effect mobility, C_i is the capacitance per unit area of the insulation layer (SiO_2, 300 nm), and V_G and V_T are the gate and threshold voltages, respectively.

The field-effect mobilities of **P1**, **P2**, and **P3** were determined to be 3×10^{-3}, 9×10^{-5}, and 7×10^{-4} cm^2 V^{-1} s^{-1}, respectively. The hole mobilities of the ester-substituted thienothiophene-based **P1** were 2 orders of magnitude higher than those of the ketone-substituted thienothiophene-based **P2**. The higher mobility measured for **P1** compared with **P2** was understood in terms of better solubility and π–π* stacking, which corresponded well to the UV-vis results. The hole mobility of **P1** was within the desired range for PSC materials (comparable to or exceeding 10^{-3} cm^2 V^{-1} s^{-1}), allowing for efficient charge extraction and a good FF. Previous reports indicated that the hole mobilities of fluorinated polymers are higher than those of unfluorinated polymers due to a higher intermolecular packing among fluorinated backbones.[30,31] In our study, no fluorine effects were observed in the field-effect carrier mobilities of the acceptor.

The hole mobility by TFTs is a "horizontal" measurement rather than the "vertical" charge transport. A method to measure the hole mobility in the vertical direction is space charge limited current (SCLC) to reveal the vertical transport in OPV device structures. To obtain the SCLC curves, the hole only devices were fabricated with the structure ITO/PEDOT:PSS/polymer/Au. As shown in the ESI,† the trend of hole mobility by SCLC is similar to that by TFTs.

Photovoltaic characteristics

Bulk-heterojunction PSCs were fabricated with the structure ITO/PEDOT:PSS/polymer:$PC_{71}BM$/Ca/Al. The device-fabrication process is described in detail in the Experimental section. The performance of PSCs was strongly affected by the processing parameters, such as the choice of solvent, blend ratio of the polymer and $PC_{71}BM$, and the additive effects. We investigated the performance of the PSC materials under a variety of conditions (see the ESI†). Optimal fabrication conditions were obtained from a 8 mg mL^{-1} solution, at a spin-coating rate of 1300 rpm, and with a polymer:$PC_{71}BM$ ratio of 1 : 1.5 (w/w). The layer thicknesses were PEDOT:PSS (40 nm), active layer (90 nm), and Ca/Al (100 nm). In agreement with the TFT properties described earlier, **P1** was found to be a suitable material for PSC applications.

Fig. 6 shows the current–voltage curves of the optimized devices based on blends of the BDT-based polymer and fullerene. The output characteristics of the resulting polymer-based devices are summarized in Table 3. Previous studies reported that the solar cell performances of benzo[1,2-*b*:4,5-*b*′]dithiophene-based polymers could be improved using a 3% 1,8-diiodooctane (DIO) to form an active layer.[30,32] We repeated the solar cell tests using **P1** either with or without the 3% DIO additive. The performance of **P1** improved in both J_{sc} and FF, yielding a maximum efficiency of 5.76% (see the ESI†). Fig. 7 shows the UV-vis absorption spectra of the **P1**:$PC_{71}BM$ films with and without the 3% DIO additive. The UV-vis spectrum of **P1** with DIO displayed well-defined sharp vibronic features compared to the

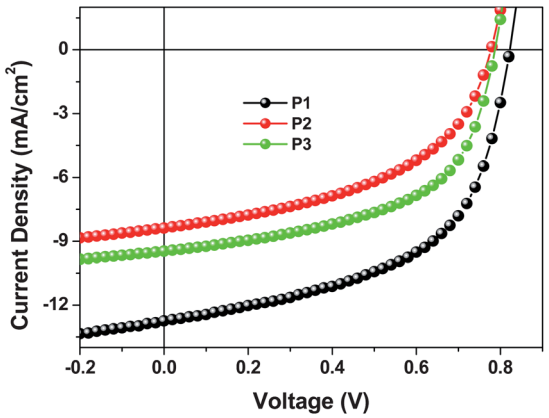

Fig. 6 *J–V* characteristics of photovoltaic devices fabricated with **P1**:$PC_{71}BM$ (black), **P2**:$PC_{71}BM$ (red), and **P3**:$PC_{71}BM$ (green) under AM 1.5 G irradiation (100 mW cm^{-2}).

Table 3 FET and PSC performances of the polymers

Polymer	Solvent	$V_{oc}{}^{b}$ (V)	$J_{sc}{}^{b}$ (mA cm^{-2})	FF^{b}	PCE^{b} (%)
P1	CB/DIO^{a}	0.82	12.75	0.55	5.76
P2	CB/DIO^{a}	0.78	8.38	0.48	3.16
P3	CB/DIO^{a}	0.79	9.47	0.55	4.11

^{a} The mixed solvent of 97% CB/3% s1,8-diiodoctane (DIO). ^{b} The device was fabricated with a layered structure of ITO/PEDOT:PSS/polymer:$PC_{71}BM$/Ca/Al.

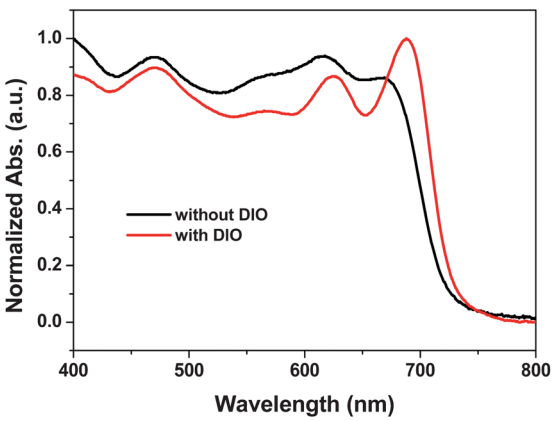

Fig. 7 UV-Vis absorption spectra of films spin coated from **P1**:$PC_{71}BM$ with or without the 1,8-diiodooctane additive.

spectrum of **P1** prepared without additives. As shown in Fig. 7, the peak in the **P1** absorption band in the **P1**:$PC_{71}BM$ composite deposited from a solution containing the additive was red-shifted by 20 nm relative to the **P1** absorption band of the film prepared without the additive. Bazan *et al.* reported that such shifts to lower energy absorption peaks are associated with a π–π^* transition if the films are processed with additives.[33,34] The red shift indicates that the **P1** chains interact more strongly and that the local structural order is higher than that in films processed from pure chlorobenzene. Under optimized conditions (97% CB/3% DIO solvent), the BDT-based polymers showed PCEs for the PSCs in the range of 3.16–5.76%. The best PSC performance

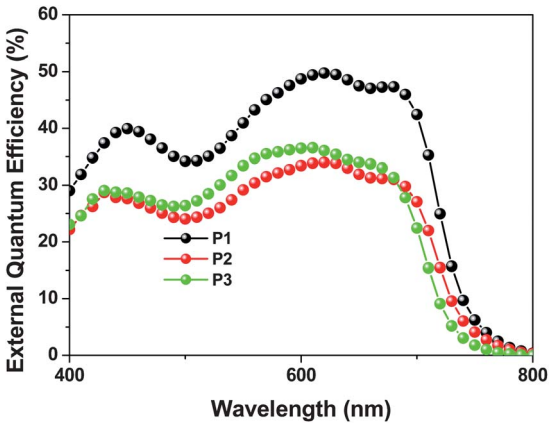

Fig. 8 External quantum efficiency of **P1**:$PC_{71}BM$ (black), **P2**:$PC_{71}BM$ (red), and **P3**:$PC_{71}BM$ (green).

was observed for **P1**:$PC_{71}BM$ devices, which reached a PCE of 5.76%, with a J_{sc} of 12.75 mA cm^{-2}, a V_{oc} of 0.82 V, and a FF of 0.55 under AM 1.5 G irradiation (100 mW cm^{-2}).

The V_{oc} value was closely related to the energy difference between the HOMO of the polymer and the LUMO of the electron acceptor, $PC_{71}BM$.[13,14] As expected from the HOMO energy levels of the polymers, all polymers exhibited similar V_{oc} values.

J_{sc} of a PSC is affected by many factors, including the absorption strength of the active layer and the charge-carrier mobility.[15,16] The values of J_{sc} measured for **P1**, **P2**, and **P3** were 12.75, 8.38, and 9.47 mA cm^{-2}, respectively. These results agreed well with the OFET measurements. As expected from the hole mobilities of the polymers (3×10^{-3} cm^2 V^{-1} s^{-1} for **P1**, 9×10^{-5} cm^2 V^{-1} s^{-1} for **P2**, and 7×10^{-4} cm^2 V^{-1} s^{-1} for **P3**), the unfluorinated ester-substituted thienothiophene-based **P1** exhibited a higher J_{sc} than the other polymers.

Fig. 8 shows the external quantum efficiency (EQE) spectra of the optimized PSC devices prepared with 3% DIO under monochromatic light illumination. The EQE spectra agreed well with the optical absorption curves, indicating that excitons were mainly generated in the polymer phase. The spectral responses of the PSC devices showed that photons within the range of 350–800 nm contributed significantly to the EQE, with a maximum EQE of 50% (at 620 nm), 34% (at 620 nm), and 37% (at 610 nm) for **P1**, **P2**, and **P3**, respectively. Convolution of the spectral response with the photon flux of the AM 1.5 G spectrum provided an estimate of the value of J_{sc} under irradiation. The calculated J_{sc} value for the **P1**, **P2**, and **P3**-based devices was 10.50, 7.17, and 7.57 mA cm^{-2}, respectively. Due to the discrepancy between the EQE results and the photon flux under AM 1.5 illumination, an approximate mismatch of 15–20% was observed between the convolution and the solar-simulator data.

Morphology plays a significant role in PSC efficiency. Fig. 9 shows atomic force microscopy (AFM) images (1 μm × 1 μm scan area) of a blend film (polymer:$PC_{71}BM$ = 1 : 1.5 in 97% CB/3% DIO solvent), in an effort to better understand the device characteristics. The surface topography (left) and phase images (right) were collected for each film and yielded insight into the device characteristics. The surface roughness values measured from the topography images were 2.05, 5.32, and 4.20 nm for **P1** (Fig. 9a), **P2** (Fig. 9c), and **P3** (Fig. 9e), respectively. A smoother

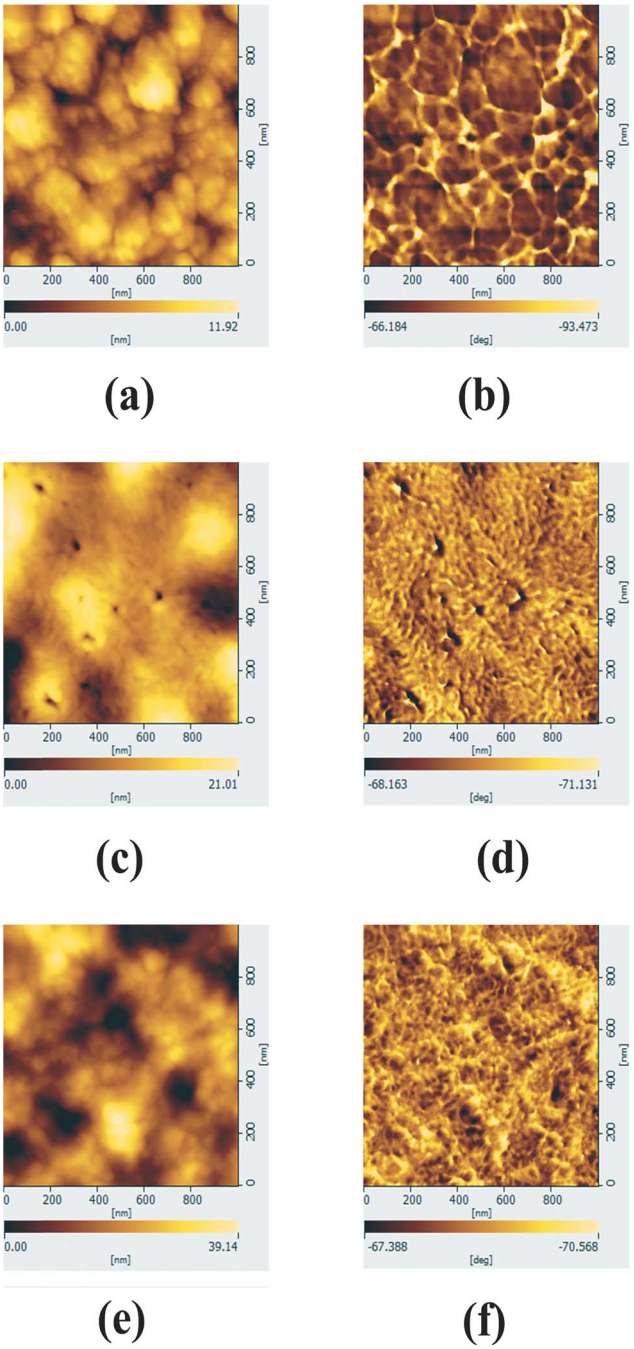

Fig. 9 AFM images of films spin-coated from **P1**:$PC_{71}BM$ (a and b), **P2**:$PC_{71}BM$ (c and d), and P3:$PC_{71}BM$ (e and f). (a, c and e) AFM topography of each film. (b, d and f) AFM phase images of each film.

active layer surface leads to an increase in the photovoltaic performances of **P1**.

Considering that the V_{oc} values of PSCs fabricated using the previously reported BDT-based copolymers with alkyl chains were found to be in the range of 0.62–0.76 V, the TIPS-substituted benzodithiophene-based copolymers showed a high V_{oc} of 0.82 V. The performance of the PSCs could potentially be greatly improved by enhancing the FF and J_{sc}. Further modifications of the polymer structure are currently underway toward achieving an even better performance.

Conclusions

In summary, a series of novel TIPS-substituted benzodithiophene-based copolymers with the same polymer backbone and different side chains were synthesized *via* Stille coupling polymerization. Although all polymers displayed similar optical and electrochemical properties, **P1** exhibited a higher hole mobility and PSC performance than the other polymers. Under optimized conditions, bulk-heterojunction solar cells fabricated from blends containing **P1** and $PC_{71}BM$ exhibited PCEs of 5.76%, with a J_{sc} of 12.75 mA cm^{-2}, a V_{oc} of 0.82 V, and a FF of 0.55. In light of the field-effect carrier mobility and photovoltaic properties of **P1**, TIPS-substituted benzodithiophene-based copolymers are promising candidates as next-generation solar cell materials. In our study, no fluorine effects were observed in the TIPS-substituted benzodithiophene-based copolymers. Also the ester-substituted thienothiophene-based **P1** exhibited higher field-effect carrier mobility and photovoltaic properties than the ketone-substituted thienothiophene-based **P2**. A preliminary experimental study of the photovoltaic performances of the TIPS-substituted BDT-based polymer was performed, and modifications of the polymer structure are in progress in an effort to achieve even better performances.

Experimental section

General

The synthesized compounds were characterized with ^1H NMR spectra obtained using a Bruker DPX-300 NMR Spectrometer. UV-visible analysis was performed with a Lambda 20 (Perkin Elmer) diode array spectrophotometer. The number- and weight-average molecular weights of the polymers were determined by gel permeation chromatography (GPC; Viscotek) equipped with a TDA 302 detector and a PL-gel (Varian) column, using chloroform as the eluent and polystyrene as the standard. Thermogravimetric analysis (TGA) was performed under a nitrogen atmosphere at a heating rate of 10 °C min^{-1} with a Dupont 9900 analyzer.

Fabrication of the organic thin film transistors (OTFTs)

OTFT devices were fabricated in a bottom-contact geometry (channel length = 12 μm, width = 120 μm). The source and drain contacts consisted of gold (100 nm), and the dielectric was silicon oxide (SiO_2) with a thickness of 300 nm. The SiO_2 surface was cleaned, dried, and pretreated with a solution of 1.0 mM octyltrichlorosilane (OTS-8) in toluene at room temperature for 2 h under nitrogen to produce apolar and smooth surfaces onto which the polymers could be spin-coated. The polymers were dissolved to a concentration of 0.5 wt% in chloroform. Films of the organic semiconductors were spin-coated at 1500 rpm for 50 s to a thickness of 50 nm, followed by an annealing process. All device fabrication procedures and measurements were carried out in air at room temperature.

Fabrication of the polymer solar cells (PSCs)

In this study, the devices were fabricated with the structure ITO/PEDOT:PSS/polymer:$PC_{71}BM$/Ca/Al. The procedure for cleaning the ITO surface included sonication and rinsing in

deionized water, methanol, and acetone. The hole-transporting PEDOT:PSS layer was spin-coated onto each ITO anode from a solution purchased from Heraeus (Clevios™ P). Each polymer:$PC_{71}BM$ solution was then spin-coated onto the PEDOT:PSS layer. $PC_{71}BM$ was purchased from Nano-C Inc. The polymer solution for spin-coating was prepared by dissolving the polymer (8 mg mL^{-1}) in 97% CB/3% 1,8-diiodooctane (DIO). Calcium and aluminum contacts were formed by vacuum deposition at pressures below 3×10^{-6} Torr, providing an active area of 0.09 cm^2. Solar cell efficiencies were characterized under simulated 100 mW cm^{-2} AM 1.5G irradiation from a Xe arc lamp with an AM 1.5 global filter. Simulator irradiance was characterized using a calibrated spectrometer, and the illumination intensity was set using an NREL-certified silicon diode with an integrated KG1 optical filter. The EQE was measured by underfilling the device area using a reflective microscope objective to focus the light output from a 100 W halogen lamp outfitted with a monochromator and an optical chopper; the photocurrent was measured using a lock-in amplifier, and the absolute photon flux was determined using a calibrated silicon photodiode. All device fabrication procedures and measurements were carried out in air at room temperature.

Materials

Triisopropylsilyl acetylene, *N*,*N*,*N*′,*N*′-tetramethyl-ethane-1,2-diamine (TMEDA), trimethyltinchloride, dimethylformamide (DMF), tetrakis(triphenylphosphine)palladium and toluene (99.8%, anhydrous) were purchased from Aldrich. All chemical were used without further purification. The monomers benzo[1,2-*b*:4,5-*b*′]dithiophene-4,8-dione,[30] 2-ethylhexyl-4,6-dibromothieno[3,4-*b*]thiophene-2-carboxylate,[16] 1-(4,6-dibromothieno[3,4-*b*]thiophen-2-yl)-2-ethylhexan-1-one,[11] 2-ethylhexyl-4,6-dibromo-3-fluorothieno[3,4-*b*]thiophene-2-carboxylate[12] were prepared by previously described methods.

4,8-Bis(triisopropylsilylethynyl)-benzo[1,2-*b*:4,5-*b*′]dithiophene (2)

To an oven-dried 500 mL round-bottom flask equipped with a stir bar and cooled to 0 °C under the protection of argon were added tetrahydrofuran (THF) (50 mL) and 6.7 mL of triisopropylsilyl acetylene (29.9 mmol), followed by the dropwise addition of 19.3 mL of *t*-BuLi (32.7 mmol, 1.7 M solution in pentane). This mixture was stirred for 2 h, then THF (120 mL) and benzo[1,2-*b*:4,5-*b*′]dithiophene-4,8-dione (5 g, 13.7 mmol) were added. The mixture was stirred at room temperature for 24 hours, and then quenched with water. The resulting mixture was poured into a saturated ammonium chloride solution and extracted with ethyl acetate (EA). The organic layer was washed with brine and dried over anhydrous $MgSO_4$. After the solvent being evaporated, the residue was dissolved in THF (120 mL), and then $SnCl_2 \cdot 2H_2O$ (15.3 g, 68.1 mmol, in 50 mL 50% acetic acid) was added dropwise. The mixture was stirred at room temperature overnight, and poured into water and extracted with EA. The organic layer was washed with sodium bicarbonate and brine, and then dried over anhydrous $MgSO_4$. Solvent was removed and the crude product was purified with column chromatography on silica with hexane as eluent, to yield **2** (3.6 g, 48%) as a light green solid. ^{1}H NMR (300 MHz, $CDCl_3$) δ (ppm) 7.61 (d, 2H), 7.56 (d, 2H), 1.23 (m, 42H). ^{13}C NMR (75 MHz, $CDCl_3$) δ (ppm) 140.86, 138.51, 128.28, 123.14, 112.18, 102.63, 101.62, 18.78, 11.33. EI-MS: *m*/*z*: 551. Anal. calcd for $C_{36}H_{46}S_2Si_2$: C, 69.75; H, 8.41; S, 11.64. Found: C, 69.71; H, 8.40; S, 11.63%.

2,6-Bis(trimethyltin)-4,8-bis(triisopropylsilylethynyl)-benzo[1,2-*b*:4,5-*b*′]dithiophene (3)

Under the protection of argon, 5.1 mL of *n*-BuLi (8.1 mmol, 1.6 M solution in hexanes) was added drop-wise *via* syringe to compound **2** (1.5 g 2.7 mmol) and TMEDA (1.2 mL, 8.1 mmol) in THF (30 mL) which was cooled at −78 °C. After stirring at low temperature for 30 minutes, 10.8 mL of trimethyltinchloride (10.8 mmol, 1 M solution in hexane) was added in one portion. The reaction mixture was allowed to warm to room temperature overnight. The reaction mixture was quenched with water then concentrated *via* rotary evaporation. The residue was diluted with chloroform, washed with brine and water. Organic layer was dried over magnesium sulfate and concentrated *via* rotary evaporation. Crude compound was recrystallized with isopropyl alcohol to yield a pale yellow solid (1.9 g, 80%). ^{1}H NMR (300 MHz, $CDCl_3$) δ (ppm) 7.69 (s, 2H), 1.23 (m, 42H). 0.47 (s, 18H). ^{13}C NMR (75 MHz, $CDCl_3$) δ (ppm) 144.68, 143.51, 139.10, 110.36, 103.33, 100.64, 19.06, 11.39, −8.3. EI-MS: *m*/*z*: 876. Anal. calcd for $C_{38}H_{62}S_2Si_2Sn_2$: C, 52.06; H, 7.13; S, 7.32. Found: C, 52.09; H, 7.11; S, 7.29%.

General procedure for the synthesis of polymers with the Stille reaction: the synthesis of poly[4,8-bis(triisopropylsilylethynyl) benzo[1,2-*b*:4,5-*b*′]dithiophene-2,6-diyl-*alt*-4,6-(2-ethylhexyl-thieno-[3,4-*b*]thiophene-2-carboxylate)] (**P1**) is presented in detail as a representative example. 2,6-Bis(trimethyltin)-4,8-bis(triisopropylsilylethynyl)-benzo[1,2-*b*:4,5-*b*′]dithiophene(262 mg, 0.3 mmol), 2-ethylhexyl 4,6-dibromothieno[3,4-*b*]thiophene-2-carboxylate (136 mg, 0.3 mmol), and $Pd(PPh_3)_4$ (14 mg, 0.04 eq.) were added into a 50 mL round-bottom flask. Then, anhydrous DMF (1 mL) and anhydrous toluene (4 mL) were added. The polymerization was carried out at 105 °C under argon protection. After 24 h, the reaction mixture was cooled to about 50 °C and added slowly to a vigorously stirred mixture consisting of 230 mL methanol and 13 mL 1 N aqueous HCl. The polymer fibers were collected by filtration and reprecipitation from methanol. The polymer was purified by washing for 2 days in a Soxhlet apparatus with acetone to remove oligomers and catalyst residues. The reprecipitation procedure in toluene–methanol was then repeated several times. The final product was obtained after drying *in vacuo* at 40 °C. ^{1}H NMR (300 MHz, $CDCl_3$) δ (pm): 8.14 (br, 1H); 7.86 (br, 1H); 7.80 (br, 1H); 4.37 (br, 2H); 1.94–0.84 (m, 57H). Anal. calcd: C, 66.93; H, 7.41; S, 15.21. Found: C, 66.91; H, 7.42; S, 15.26%.

Poly[4,8-bis(triisopropylsilylethynyl)benzo[1,2-*b*:4,5-*b*′]dithiophene-2,6-diyl-*alt*-[4,6-{(1-thieno[3,4-*b*]thiophen-2-yl)-2-ethylhexan-1-one}] (**P2**) was synthesized with the procedure described for **P1**. The copolymerization of the monomers 2,6-bis-(trimethyltin)-4,8-bis(triisopropylsilylacetylene)-benzo[1,2-*b*:4,5-*b*′]dithiophene (262 mg, 0.3 mmol) and 1-(4,6-dibromothieno[3,4-*b*]thiophen-2-yl)-2-ethylhexan-1-one (126 mg, 0.3 mmol) gave **P2** (84%). ^{1}H NMR (300 MHz, $CDCl_3$) δ (pm): 7.98 (br, 1H);

7.76 (br, 1H); 7.72 (br, 1H); 3.26 (br, 1H); 1.94–0.72 (m, 56H). Anal. calcd: C, 67.92; H, 7.44; S, 15.77. Found: C, 67.87; H, 7.51; S, 15.78%.

Poly[4,8-bis(triisopropylsilylethynyl)benzo[1,2-*b*:4,5-*b*′]dithiophene-2,6-diyl-*alt*-4,6-(2-ethylhexyl(3-fluorothieno[3,4-*b*]thiophene)-2-carboxylate)] (**P3**) was synthesized with the procedure described for **P1**. The copolymerization of the monomers 2,6-bis(trimethyltin)-4,8-bis(triisopropylsilylacetylene)-benzo[1,2-*b*:4,5-*b*′]dithiophene (262 mg, 0.3 mmol) and 2-ethylhexyl 4,6-dibromo-3-fluorothieno[3,4-*b*]thiophene-2-carboxylate (140 mg, 0.3 mmol) gave **P3** (87%).^{1}H NMR (300 MHz, $CDCl_3$) δ (pm): 7.96 (br, 1H); 7.70 (br, 1H); 4.28 (br, 2H); 1.86–0.80 (m, 57H). Anal. calcd: C, 65.53; H, 7.14; S, 14.89. Found: C, 65.43; H, 7.11; S, 14.83%.

Acknowledgements

This study was supported by the Converging Research Center Program through the Ministry of Education, Science and Technology (2011K000585) and by a grant from the cooperative R&D Program funded by the Korea Research Council Industrial Science and Technology, Republic of Korea. This research at the University of Ulsan was supported by the Basic Science Research Program (2011-0009148) and the Priority Research Centers Program (2009-0093818) through the NRF of Korea funded by the MEST.

References

1 S. H. Park, A. Roy, S. Beaupre, S. Cho, N. Coates, J. S. Moon, D. Moses, M. Leclerc, K. Lee and A. J. Heeger, *Nat. Photonics*, 2009, **3**, 297.
2 Y. D. Park, J. K. Park, W. H. Lee, B. Kang, K. Cho and G. C. Bazan, *J. Mater. Chem.*, 2012, **22**, 11462.
3 T. Tromholt, M. V. Madsen, J. E. Carle, M. Helgesen and F. C. Krebs, *J. Mater. Chem.*, 2012, **22**, 7592.
4 C. Duan, F. Huang and Y. Cao, *J. Mater. Chem.*, 2012, **22**, 10416.
5 J. K. Park, J. Jo, J. H. Seo, J. S. Moon, Y. D. Park, K. Lee, A. J. Heeger and G. C. Bazan, *Adv. Mater.*, 2011, **23**, 2430.
6 S. K. Lee, J. M. Cho, Y. Goo, W. S. Shin, J.-C. Lee, W.-H. Lee, I.-N. Kang, H.-K. Shim and S.-J. Moon, *Chem. Commun.*, 2011, **47**, 1791.
7 M. Zhang, X. Guo, X. Wang, H. Wang and Y. Li, *Chem. Mater.*, 2011, **23**, 4264.
8 S. K. Lee, W.-H. Lee, J. M. Cho, S. J. Park, J.-U. Park, W. S. Shin, J.-C. Lee, I.-N. Kang and S.-J. Moon, *Macromolecules*, 2011, **44**, 5994.
9 Y. Zhang, J. Zou, H.-L. Yip, K.-S. Chem, D. F. Zeigler, Y. Sun and A. K.-Y. Jen, *Chem. Mater.*, 2011, **23**, 2289.
10 S. K. Lee, S. Cho, M. Tong, J. H. Seo and A. J. Heeger, *J. Polym. Sci., Part A: Polym. Chem.*, 2011, **49**, 1821.
11 H.-Y. Chem, J. H. Hou, S. Q. Zhang, Y. Liang, G. W. Yang, Y. Yang, L. P. Yu, Y. Wu and G. Li, *Nat. Photonics*, 2009, **3**, 649.
12 Y. Liang, Z. Xu, J. Xia, S.-T. Tsai, Y. Wu, G. Li, C. Ray and L. Yu, *Adv. Mater.*, 2010, **22**, E135.
13 S. J. Park, J. M. Cho, W.-B. Byun, J.-C. Lee, W. S. Shin, I.-N. Kang, S.-J. Moon and S. K. Lee, *J. Polym. Sci., Part A: Polym. Chem.*, 2011, **49**, 4416.
14 G. Dennler, M. C. Scharber, T. Ameri, P. Denk, K. Forberich, C. Waldauf and C. J. Brabec, *Adv. Mater.*, 2008, **20**, 579.
15 C. Melzer, E. J. Koop, V. D. Mihailetchi and P. W. M. Blom, *Adv. Funct. Mater.*, 2004, **14**, 865.
16 Y. Liang, Y. Wu, D. Feng, S.-T. Tsai, H.-J. Son, G. Li and L. Yu, *J. Am. Chem. Soc.*, 2009, **131**, 56.
17 H. Ohkita, S. Cook, Y. Astuti, W. Duffy, S. Tierney, W. Zhang, M. Heeney, I. McCulloch, J. Nelson, D. D. C. Bradley and J. R. Durrant, *J. Am. Chem. Soc.*, 2008, **130**, 3030.
18 S. C. Price, A. C. Stuart and W. You, *Macromolecules*, 2010, **43**, 4609.
19 Y. Li, L. Xue, H. Li, Z. Li, B. Xu, S. Wen and W. Tian, *Macromolecules*, 2009, **42**, 4491.
20 Y. Zhang, J. Zou, H.-L. Yip, K.-S. Chen, J. A. Davis, Y. Sun and A. K.-Y. Jen, *Macromolecules*, 2011, **44**, 4752–4758.
21 Y. Zhang, J. Zou, H.-L. Yip, Y. Sun, J. A. Davis, K.-S. Chen, O. Acton and A. K.-Y. Jen, *J. Mater. Chem.*, 2011, **21**, 3895–3902.
22 J.-H. Park, D. S. Chung, D. H. Lee, H. Kong, I. H. Jung, M.-J. Park, N. S. Cho, C. E. Park and H.-K. Shim, *Chem. Commun.*, 2010, **46**, 1863.
23 Q. Shi, H. Fan, Y. Liu, W. Hu, Y. Li and X. Zhan, *Macromolecules*, 2011, **44**, 9173.
24 A. Gadisa, W. Mammo, L. M. Andersson, S. Admassie, F. Zhang, M. R. Andersson and O. Inganas, *Adv. Funct. Mater.*, 2007, **17**, 3836.
25 H. J. Son, W. Wang, T. Xu, Y. Liang, Y. Wu, G. Li and L. Yu, *J. Am. Chem. Soc.*, 2011, **133**, 1885.
26 S. K. Lee, N. S. Cho, S. Cho, S.-J. Moon, J. K. Lee and G. C. Bazan, *J. Polym. Sci., Part A: Polym. Chem.*, 2009, **47**, 6873.
27 K. M. Coakley and M. D. McGehee, *Chem. Mater.*, 2004, **16**, 4533.
28 S. K. Lee, I.-N. Kang, J.-C. Lee, W. S. Shin, W.-W. So and S.-J. Moon, *J. Polym. Sci., Part A: Polym. Chem.*, 2011, **49**, 3129.
29 W.-H. Lee, S. K. Son, K. Kim, S. K. Lee, W. S. Shin, S.-J. Moon and I.-N. Kang, *Macromolecules*, 2012, **45**, 1303.
30 Y. Liang, D. Feng, Y. Wu, S.-T. Tsai, G. Li, C. Ray and L. Yu, *J. Am. Chem. Soc.*, 2009, **131**, 7792.
31 Y. Zhang, S.-C. Chien, K.-S. Chen, H.-L. Yip, Y. Sun, J. A. Davies, F.-C. Chen and A. K.-Y. Jen, *Chem. Commun.*, 2011, **47**, 11026–11028.
32 Q. Peng, X. Liu, D. Su, G. Fu, J. Xu and L. Dai, *Adv. Mater.*, 2011, **23**, 4554.
33 J. Peet, J. Y. Kim, N. E. Coates, W. L. Ma, D. Moses, A. J. Heeger and G. C. Bazan, *Nat. Mater.*, 2007, **6**, 497.
34 J. K. Lee, W. L. Ma, C. J. Brabec, J. Yuen, J. S. Moon, J. Y. Kim, K. Lee, G. C. Bazan and A. J. Heeger, *J. Am. Chem. Soc.*, 2008, **130**, 3619.

